THE JOURNAL OF PHYSICAL CHEMISTRY B

ARTICLE

pubs.acs.org/JPCB

Systematic Investigation of the Catalytic Cycle of a Single Site Ruthenium Oxygen Evolving Complex Using Density Functional Theory

Thomas F. Hughes and Richard A. Friesner*

Department of Chemistry, Columbia University, New York, New York 10027, United States

ABSTRACT: The mechanism of water oxidation by a single site ruthenium oxygen evolving complex is investigated using fully unrestricted pseudospectral B3LYP with the effective core potential LACV3P in continuum solvent with some quantum mechanical waters. Guess wave functions have been used that allow greater flexibility in sampling different electronic configurations of the complex. Systematic comparison with experiment is improved using these guesses because they provide a complete analysis of the low energy manifold and help to alleviate the formal disconnect between theory and experiment in assigning Lewis structures for transition metal complexes. In agreement with results from the literature, the challenging $4e^-$ and $4H^+$ oxidation of water is accomplished using a mechanism that features three proton coupled electron transfers, one electron transfer, one atom proton transfer (APT), and one ligand exchange (LE). Calculations on a large database of ruthenium complexes allows us to benchmark the computation of reduction half potentials and free energies of activation and to investigate systematic ligand variations and their effect on the reaction mechanism. Mean unsigned errors of reduction half potentials in comparison to experiment are generally small (100−200 mV). The APT and LE steps are found to be rate limiting with free energy barriers of 19.27 and 19.53 kcal/mol respectively, which is in excellent agreement with the ∼20 kcal/mol barrier obtained from experimental rate constants using classical transition state theory.

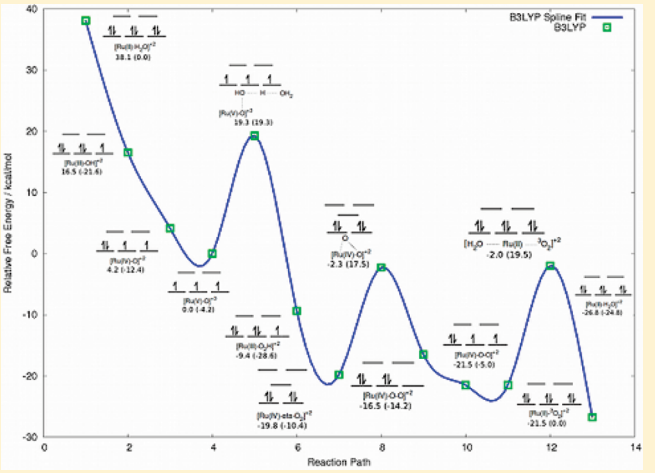

1. INTRODUCTION

Two to three billion years ago green plants learned through evolution how to take sunlight and produce oxygen using a water oxidation mechanism known to be one of the most energetically demanding biological redox processes on Earth because it requires removal of $4e^-$ and $4H^+$ and creation of an oxygen−oxygen bond.[1−4] Yet it occurs at rates and efficiencies that are large enough to sustain the life of aerobic organisms. Despite ongoing debate about the exact structure of the oxygen evolving complex (OEC) in photosystem II, the core of which contains 4 Mn atoms and 1 Ca atom, and its water oxidation mechanism, it is generally believed that the reaction occurs through a high oxidation state manganese-oxo intermediate which is the catalytically competent species produced by successive proton coupled electron transfers (PCETs).[5−8] The proposed mechanism for single site ruthenium water oxidation involves a high oxidation state ruthenium-oxo intermediate, $[Ru(V)=O]^{+3}$, also the catalytically competent species produced by successive PCETs.[6,9−15] An efficient and inexpensive water oxidation reaction introduces the prospect of "clean energy" because hydrogen gas can easily be obtained from the proton gradient of a given cell, mixed with oxygen from the atmosphere, and combusted to do work, leaving water as the only product. A successful synthetic catalyst would need to be easily regenerated with high turnover frequencies much like the natural catalysts whose properties they are meant to emulate.

Many synthetic catalysts have been developed to carry out artificial photosynthesis;[16−22] however, none of them approach the rate and efficiency of photosystem II.[6] It was recently discovered that single site ruthenium complexes[6,9−15,22,23] with a variety of ligands, for example polypyridyl, acac, carbenes, water, chloride, carboxyl, etc., serve as a competitive prototype to other synthetic OECs including its predecessor the ruthenium blue dimer[10,24−29] which has been of great interest for many years. Although the focus of this work is on single site ruthenium water oxidation catalysis other recently developed catalysts include nonruthenium transition metal complexes made from the first, i.e., manganese,[30,31] iron,[32] and cobalt;[33,34] second, i.e., molybdenum;[35] and third, i.e., iridium,[36] rows of the periodic

Received: March 21, 2011
Revised: June 7, 2011
Published: June 16, 2011

table's d-block, as well as approaches using polymers[37] and those that are more biological.[38] Single site catalysts are beneficial for a number of reasons including that they are generally small molecules and thus amenable to a greater variety of experiments. Originally it was hypothesized that the oxygen evolution from single site ruthenium complexes was in fact due to ruthenium dioxide nanoparticles formed by the decomposition of the single site catalysts. A series of systematic experiments has recently shown that it is the single site ruthenium complex which is in fact responsible for oxygen evolution.[23,39] In principle, with a greater understanding of the underlying reaction mechanism, the properties of these complexes can be tuned to give a catalytic time-scale of milliseconds as opposed to hours.[6,10,15,23]

A number of pH dependent cyclic voltammetry and kinetics experiments have led to a good initial understanding of the chemistry of the single site ruthenium complexes discussed in ref 10; the proposed mechanism for water oxidation is summarized in Meyer et al.'s Figure 1.[6,10] Successively, it features two PCETs, electron transfer (ET), atom proton transfer (APT), another PCET, and ligand exchange (LE)

$$[\mathrm{Ru(III)-OH}]^{+2} + e^- + H^+ \rightarrow [\mathrm{Ru(II)-H_2O}]^{+2} \quad (1)$$

$$[\mathrm{Ru(IV)-O}]^{+2} + e^- + H^+ \rightarrow [\mathrm{Ru(III)-OH}]^{+2} \quad (2)$$

$$[\mathrm{Ru(V)-O}]^{+3} + e^- \rightarrow [\mathrm{Ru(IV)-O}]^{+2} \quad (3)$$

$$[\mathrm{Ru(V)-O}]^{+3} + 2H_2O \rightarrow [\mathrm{Ru(III)-OOH}]^{+2} + H_3O^+ \quad (4)$$

$$[\mathrm{Ru(IV)-O_2}]^{+2} + e^- + H^+ \rightarrow [\mathrm{Ru(III)-OOH}]^{+2} \quad (5)$$

$$[\mathrm{Ru(IV)-O_2}]^{+2} + H_2O \rightarrow [\mathrm{Ru(II)-H_2O}]^{+2} + O_2 \quad (6)$$

where the redox reactions are shown as reduction half potentials and from this point forth all metal ligand bonds are simply represented as a single dash (despite the possibility of doubly bonded moieties as in $[\mathrm{Ru(V)=O}]^{+3}$, for a brief discussion of bonding in, for example, *cis* $-$ $[\mathrm{Ru(II)}(bpy)_2(\mathrm{H_2O})_2]^{+2}$ see ref 39). The net water oxidation reaction involving the transfer of $4e^-$ is,

$$2H_2O + 4Ce^{+4} \rightarrow O_2 + 4H^+ + 4Ce^{+3} \quad (7)$$

Ce^{4+} is used as the sacrificial oxidizing agent[10] because with its large reduction half potential of 1.76 V it can oxidize the resting state catalyst, $[\mathrm{Ru(II)-H_2O}]^{+2}$, all the way up to the catalytically competent species, $[\mathrm{Ru(V)-O}]^{+3}$, where ruthenium has a large oxidation state.

The largest cyclic voltammetry wave is pH independent and assigned as the ET event that creates the catalytically competent species while the other pH dependent waves are assigned as PCETs.[11] APT (eq 4) and LE (eq 6) reactions are rate limiting. The APT involves nucleophilic attack by water on the activated oxo ligand of $[\mathrm{Ru(V)-O}]^{+3}$ coupled with simultaneous transfer of a proton to a base. Herein this base is assumed to be water however as recently shown[6,40] changes in base strength can have a drastic effect on the barriers of the APT step. Kinetic isotope effects show that the APT step involves a single proton mechanism. Other kinetics experiments show that the rate is first order in ruthenium complex and that the water oxidation is catalyzed using a single metal center.[12] Less is known experimentally about the rate limiting oxygen evolution step, however some calculations show that there is a barrier in going from $[\mathrm{Ru-}\eta^2\mathrm{-O_2}]^{+2}$ to $[\mathrm{Ru-O-O}]^{+2}$ prior to oxygen release[12] as well as a barrier for the LE step involving a hepta-coordinate transition state.[14] Additionally, in order to produce ground state $^3O_2$ gas, two electrons must be transferred from the ligand to the metal.

Depending on the ligands, the rate determining steps have 15−60 min experimental half-lives,[11] which are far from the desired millisecond range. Activation free energies have been reduced using three techniques, the first being the use of strong bases to assist proton transfer in the APT step shown in eqs 4 and 6, the second being synthetic modifications to increase the electron donating character of the ligands (for example as in the series bpy (2,2′-bipyridine), bpm (2,2′-bipyrimidine), and bpz (2,2′-bipyrazine)[11]), and the third being the use of nonaqueous solvents where water is a limiting reagent.[40] The first approach shows that the rate constants can be increased by 4 orders of magnitude when using strong bases such as HPO_4^{-2} ($pK_a^{H_2PO_4^{-2}}$ 7.20) compared to water ($pK_a^{H_3O^+}$ −1.74). Unfortunately, the problem with this approach is that anation makes it difficult to free up catalyst.[6] Using the synthetic modification approach reduces the reaction half-lives from 60 min (bpy) to 15 min (bpm) and finally to 8 min (bpz).[11] Recently, it was shown that a significant increase in the rate of catalysis can be obtained in organic solvents where water is a limiting reagent, i.e. as the catalyst is found in the membrane embedded OEC of photosystem II. Here choice of solvent is important because organic solvent molecules can take the place of water as a coordinating ligand thereby halting progress in creating the catalytically competent $[\mathrm{Ru(V)-O}]^{+3}$ species.[40] The water oxidation rate increases as the concentration of water in propylene carbonate increases up to the point of immiscibility relative to the same catalyst in aqueous solution of low pH. In propylene carbonate, which is a weaker base than water, and water mixtures there is a much smaller kinetic isotope effect than in water alone suggesting a single water molecule attacking the activated oxygen of ruthenium with no proton transfer giving a peroxidic species. Unfortunately under certain conditions the oxygen evolution rate enhancement seen in propylene carbonate and water mixtures is diminished due to competing reductive pathways that form peroxidic species from $[\mathrm{Ru(IV)-O_2}]^{+2}$ rather than regenerating resting state catalyst and releasing O_2.[40]

Quantum chemical approaches have been used to study both the single site ruthenium and blue dimer water oxidation mechanisms.[6,10,14,27,41−47] As is well-known, density functional theory (DFT) calculations on transition metal complexes can be quite challenging. Depending on the desired property, the results can be sensitive to both basis set and functional. For example, different functionals can give qualitatively different wave functions that predict different ground state multiplicities of transition metal complexes as well as different spin-splittings, redox potentials, bond dissociation energies, etc.[48−63] In addition to problems with the DFT model, there can also be significant difficulties in converging calculations to the correct low energy electronic state for a particular system of a given multiplicity. Many challenging problems of this type can be successfully addressed with a complete search of the low energy manifolds using a series of guess wave functions that give flexibility in sampling different electron configurations for the d-orbital manifold.[64,65]

A complete analysis of a catalytic cycle with sufficient understanding to suggest the synthetic modifications needed to

improve efficiency necessitates detailed knowledge of the electronic structure for various intermediates and their state to state conversions. A valence bond type of expansion can be envisioned for a given chemotype, for example $[Ru-O_2]^{+2}$, in terms of resonance contributors, i.e., various oxidation states and multiplicities of ruthenium complexed with different electronic structures for O_2, for example triplet O_2, singlet O_2, singlet O_2^{-2}, doublet superoxide O_2^{-1}, etc. Sampling all of these electronic degrees of freedom combined with simultaneous sampling of different nuclear degrees of freedom, for example different coordinating ligands and their protonation states, can become a large project very quickly, yet there is often great regularity in results among a database of transition metal complexes calculated in this way.[66] Automated procedures thereby become imperative and appropriate tools can easily be assembled using the Python API of Maestro.[67] With this protocol, a greater degree of understanding of the electronic structure and energetics, for a given target problem, may be achieved because the results of a very large number of calculations can be systematically clustered and discriminated, resulting in much less noise than conventional procedures.

In previous work, we have utilized calculations employing comprehensive searches of the low energy state space to investigate the performance of the B3LYP[68,69] functional for various properties of transition metal complexes, including bond energies of small species (e.g., diatomics)[70] and spin-splittings of octahedral complexes of first row transition metals.[66] In these cases, systematic error patterns were uncovered, and empirical corrections, based on our DFT-LOC (localized orbital correction) approach, were shown to dramatically lower errors for a large and diverse experimental data set. The present paper is focused on the specific application of our approach to modeling the catalytic cycle of oxygen evolution by the single site ruthenium catalysts discussed above. The paper is divided into two types of studies. In the first, we compute ET and PCET reduction half potentials for a large set of relevant ruthenium containing species and compare the results with experimental data obtained from cyclic voltammetry. These results display relatively modest errors and, hence, validate the use of B3LYP for investigation of the reactions in the catalytic cycle. In the second component of the paper, we provide a thermodynamic analysis of every intermediate in the cycle and investigate in detail the reaction barriers for the rate limiting steps, which can be directly compared with experiment.

The mean unsigned errors (MUEs) with respect to experiment of ET and PCET reduction half potentials for some transition metal complexes are typically small, 100−200 mV (2−5 kcal/mol), however larger errors can occur.[14,27,60−63] Some redox processes are coupled with spin-crossover, however, there are three factors that result in a large ligand field splitting energy, Δ_o, for the various intermediates in the catalytic cycle discussed above (1) ruthenium is in the fifth row of the periodic table, (2) ruthenium typically has a high oxidation state, and (3) the coordinating aromatic nitrogens and other ligands are of intermediate interaction strength with the metal, as opposed to weakly interacting, according to the spectrochemical series.

In the present paper we analyze the entire catalytic cycle of the single site ruthenium OEC studied in.[6,10−13] Our calculation protocol is discussed in the Methods section. In section 3.1 we discuss the B3LYP computation of a benchmark database of PCET reduction half potentials for ruthenium complexes. These results, which display very good agreement with experiment, suggest as noted above that B3LYP is a suitable functional with which to analyze the present catalytic cycle, a conclusion that should not be taken for granted. In sections 3.2 and 3.3 we discuss the catalytic cycle of single site ruthenium OEC, first the PCET and ET steps and second the APT and LE steps. In section 3.4 we present a complete set of results for the energetics with a free energy diagram. Finally in the conclusion, we summarize the main points of the paper.

2. METHODS

All calculations were done using Jaguar version 7.5[65] with the relativistic effective core potential LACV3P, a triple-ζ contraction of the LACVP[71] basis set for metal centers, and 6-311G for the rest of the atoms. This basis set was chosen because it has been shown in the literature to work well in many standard B3LYP applications to metal containing systems.[70,72,73] Previous work has shown that while there is some basis set dependence, for certain properties, the differences in average error between results obtained using the medium (LACV3P) and very large (QZVP(-g)) basis sets are generally small. Fully unrestricted pseudospectral B3LYP[74] has been used with water as a continuum solvent modeled using the Poisson−Boltzmann solver in Jaguar[65] along with some quantum mechanical waters as appropriate. Due to the high quality of the chosen solvation model, we have found only minor changes in the free energies of activation when including solvation shells, consisting of up to three quantum mechanical waters, around the reaction centers. Configuration sampling of ligands and waters was performed using simple scripts written with the Python API of Maestro.[67] Many geometry minimization calculations used initial geometries from X-ray crystal structures.

As recently discussed,[66] initial guess density matrices are used which are based on a fragmentation scheme to assign atomic formal charges and multiplicities and where the metal guess comes from ligand field theory considerations.[64,65] Proper sampling of electron configurations for the d-orbital manifold is then obtained, i.e., by considering all permutations of singly and doubly occupied t_{2g} and e_g orbitals. These guesses help to alleviate some of the difficulties that quantum chemical methods have with convergence to the correct states of transition metal complexes and are useful for exploring the resonance contributors.

Reduction half potentials are calculated using the following equations. For the general multiple PCET reduction half reaction

$$A + n_e e^- + n_H H^+ \rightarrow AH_{n_H}^{(n_H - n_e)} \quad (8)$$

the standard reduction half potential (assuming $n_H = 0$), $E^0_{1/2}$, is related to the standard electron attachment (EA) free energy of solvation, ΔG^0_{EA},[27,63] by

$$\Delta G^0_{EA} = G^0(A^{-n_e}) - G^0(A) \quad (9)$$

$$\Delta G^0_{EA} = \Delta G^0_{1/2} = -n_e F E^0_{1/2} \quad (10)$$

where solvation superscripts are assumed throughout and F is the Faraday constant. For nonzero n_H we have

$$\Delta G^0_{1/2} = G^0(AH_{n_H}^{(n_H - n_e)}) - G^0(A) - n_H G^0(H^+) \quad (11)$$

where $G^0(H^+) = -11.64$ V is the solvation free energy of a proton. The dependence of the reduction half potential on

Table 1. Comparison of Experimental[76] and DFT PCET Reduction Half Potentials for the (III/II) Couple of a Variety of Ruthenium Complexes[a]

	$E_{1/2}$(III/II)/V				
resting state complex	exp.	lit.	exp.-lit.	B3LYP	exp.-B3LYP
$[Ru(II)(tpy)(acac)(H_2O)]^{+}$	0.84	0.62	0.22	0.80	0.04
$[Ru(II)(tpy)(C_2O_4)(H_2O)]$	0.81	0.46	0.35	0.73	0.08
$[Ru(II)(tpy)(H_2O)_3]^{+2}$	0.82	0.75	0.08	0.84	−0.02
trans-$[Ru(II)(tpy)(pic)(H_2O)]^{+}$	0.86	0.68	0.18	0.87	−0.01
cis-$[Ru(II)(tpy)(pic)(H_2O)]^{+}$	1.03	0.81	0.22	1.02	0.01
cis-$[Ru(II)(6,6'\text{-}Me_2bpy)_2(H_2O)_2]^{+2}$	1.04	0.92	0.13	1.00	0.04
$[Ru(II)(tpy)(tmen)(H_2O)]^{+2}$	1.01	0.85	0.16	1.00	0.01
$[Ru(II)(tpy)(phen)(H_2O)]^{+2}$	1.15	0.92	0.23	1.07	0.08
cis-$[Ru(II)(bpy)_2(Py)(H_2O)]^{+2}$	1.07	0.85	0.22	0.96	0.11
$[Ru(II)(tpy)(bpy)(H_2O)]^{+2}$	1.14	0.94	0.20	1.06	0.08
$[Ru(II)(tpy)(4,4'\text{-}(CO_2Et)_2bpy)(H_2O)]^{+2}$	1.31	1.04	0.27	1.17	0.14
$[Ru(II)(tpy)(4,4'\text{-}Me_2bpy)(H_2O)]^{+2}$	1.12	0.94	0.18	1.02	0.10
cis-$[Ru(II)(bpy)_2(AsPh_3)(H_2O)]^{+2}$	1.15	0.79	0.37	0.99	0.16
cis-$[Ru(II)(bpy)(biq)(PEt_3)(H_2O)]^{+2}$	1.10	0.84	0.26	1.00	0.10
$[Ru(II)(tpm)(4,4'\text{-}(NO_2)_2bpy)(H_2O)]^{+2}$	1.21	1.06	0.15	1.18	0.03
cis-$[Ru(II)(bpy)_2(PEt_3)(H_2O)]^{+2}$	1.11	0.88	0.23	0.97	0.14
cis-$[Ru(II)(bpy)(biq)(P(Ph_3)(H_2O)]^{+2}$	1.13	0.84	0.29	1.10	0.03
cis-$[Ru(II)(bpy)_2(P(i\text{-}Pr)_3)(H_2O)]^{+2}$	1.10	0.78	0.32	0.99	0.11
cis-$[Ru(II)(bpy)_2(SbPh_3)(H_2O)]^{+2}$	1.17	0.70	0.47	1.01	0.16
cis-$[Ru(II)(bpy)_2(P(Ph)_3)(H_2O)]^{+2}$	1.15			0.98	0.17

[a] DFT calculations are explained in the text. Literature DFT results are in the Supporting Information of ref 14.

pH is given by the Nernst equation where nonstandard $E_{1/2}$ is calculated using the following equation assuming standard states for both A and $AH_{n_H}^{(n_H-n_e)}$

$$E_{1/2} = -\left(\frac{\Delta G^0_{1/2}}{n_e}\right) - \frac{RT\ln(10)n_H}{n_e}\mathrm{pH} - E^{0,\mathrm{ref}}_{1/2} \qquad (12)$$

where $E^{0,\mathrm{ref}}_{1/2}$ is the reference potential (usually either normal hydrogen electrode (NHE) at 4.44 V or the standard calomel electrode (SCE) at 0.24 V relative to NHE).[63] For a single PCET the pH dependent term is 0.06 V per pH unit.

Transition state searches were performed using analytic second derivatives with linear and quadratic synchronous transit methods[75] and a variety of mode following techniques.[65] In a few cases the full quantum mechanical Hessian was used. The following strategy is beneficial for transition state searches in large systems. Starting with a simplified model of a given complex, for example in which certain ligands are removed or truncated, possibly with the removal of the metal as well, standard transition state methods are used to find the transition state. Next, one or a small number of chemical groups are returned to the model complex (thereby bringing it closer to the final target complex) followed by constrained geometry minimization over the most recently added degrees of freedom. Next, a standard unconstrained transition state search is performed. This protocol of constrained minimization followed by unconstrained transition state search is carried out as we build up the target complex. All minimum energy path calculations were done adiabatically, are density and Hessian followed, and are done for both the forward and reverse reactions using a number of initial guesses.

3. RESULTS AND DISCUSSION

3.1. Benchmark Database of B3LYP PCET Reduction Half Potentials for Ruthenium Complexes. PCET reduction half potentials have been computed for the (III/II) and (IV/III) couples of a large database of ruthenium complexes and compared to both experiment[76] and literature DFT results.[14] The (III/II) (like eq 1) and (IV/III) (like eq 2) couples are shown in Tables 1 and 2 respectively and have rather large positive values in comparison to some other metal complexes.[63] Literature DFT[14] results for the *cis*-$[Ru(II)(bpy)_2(P(Ph)_3)(H_2O)]^{+2}$ complex were not provided. Using our calculation protocol, the B3LYP results are consistently about 100 mV less than the experimental results which is about the same magnitude and sign as the error obtained in many other transition metal complexes.[63] Considering the changes in the electronic structure given that the PCETs involve both proton and electron attachment as well as given the great variety of coordinating ligands, it is remarkable that the B3LYP results display such small and systematic errors. The average MUE for the literature DFT results[14] is 240 mV with a standard deviation of 90 mV while our protocol results in a MUE of 80 mV with a standard deviation of 50 mV. For the (IV/III) couple shown in Table 2 the MUE for the literature DFT results is 120 mV with a standard deviation of 100 mV while our protocol gives a MUE of 110 mV with a standard deviation of 80 mV. In this case the errors for the derivatized triphenylphosphine complexes, toward the bottom of Table 2, are slightly larger.

The (III/II) reduction couple, Table 1, shows that ruthenium in the reactant, $[Ru(III)-OH]^{+2}$, has a doublet $t^2_{2g}t^2_{2g}t^1_{2g}$ electron configuration while ruthenium in the product (resting state), $[Ru(II)-H_2O]^{+2}$, has a singlet $t^2_{2g}t^2_{2g}t^2_{2g}$ electron configuration. Note that in this paper all redox reactions are considered as

Table 2. Comparison of Experimental[76] and DFT PCET Reduction Half Potentials for the (IV/III) Couple of a Variety of Ruthenium Complexes[a]

	$E_{1/2}$(IV/III)/V				
resting state complex	exp.	lit.	exp.-lit.	B3LYP	exp.-B3LYP
$[Ru(II)(tpy)(acac)(H_2O)]^{+}$	1.21	1.03	0.18	1.06	0.15
$[Ru(II)(tpy)(C_2O_4)(H_2O)]$	1.10	0.94	0.16	1.00	0.10
$[Ru(II)(tpy)(H_2O)_3]^{+2}$	1.11	1.12	0.00	1.12	−0.01
trans-$[Ru(II)(tpy)(pic)(H_2O)]^{+}$	1.10	1.00	0.10	0.99	0.11
cis-$[Ru(II)(tpy)(pic)(H_2O)]^{+}$	1.21	1.13	0.08	1.16	0.05
cis-$[Ru(II)(6,6'\text{-}Me_2bpy)_2(H_2O)_2]^{+2}$	1.20	1.18	0.03	1.23	−0.03
$[Ru(II)(tpy)(tmen)(H_2O)]^{+2}$	1.24	1.21	0.03	1.13	0.11
$[Ru(II)(tpy)(phen)(H_2O)]^{+2}$	1.25	1.25	0.00	1.25	0.00
cis-$[Ru(II)(bpy)_2(Py)(H_2O)]^{+2}$	1.18	1.32	−0.14	1.24	−0.06
$[Ru(II)(tpy)(bpy)(H_2O)]^{+2}$	1.27	1.25	0.02	1.24	0.03
$[Ru(II)(tpy)(4,4'\text{-}(CO_2Et)_2bpy)(H_2O)]^{+2}$	1.45	1.26	0.19	1.27	0.18
$[Ru(II)(tpy)(4,4'\text{-}Me_2bpy)(H_2O)]^{+2}$	1.26	1.23	0.03	1.24	0.02
cis-$[Ru(II)(bpy)_2(AsPh_3)(H_2O)]^{+2}$	1.32	1.18	0.14	1.21	0.11
cis-$[Ru(II)(bpy)(biq)(PEt_3)(H_2O)]^{+2}$	1.28	1.15	0.13	1.15	0.13
$[Ru(II)(tpm)(4,4'\text{-}(NO_2)_2bpy)(H_2O)]^{+2}$	1.40	1.40	0.00	1.41	−0.01
cis-$[Ru(II)(bpy)_2(PEt_3)(H_2O)]^{+2}$	1.32	1.20	0.12	1.18	0.14
cis-$[Ru(II)(bpy)(biq)(P(Ph_3)(H_2O)]^{+2}$	1.35	1.01	0.34	1.12	0.23
cis-$[Ru(II)(bpy)_2(P(i\text{-}Pr)_3)(H_2O)]^{+2}$	1.33	1.01	0.32	1.14	0.19
cis-$[Ru(II)(bpy)_2(SbPh_3)(H_2O)]^{+2}$	1.45	1.22	0.23	1.19	0.27
cis-$[Ru(II)(bpy)_2(P(Ph)_3)(H_2O)]^{+2}$	1.41			1.21	0.20

[a] DFT calculations are explained in the text. Literature DFT results are in the Supporting Information of ref 14.

standard reductions despite the fact that the single site ruthenium OEC in fact goes through a series of oxidations in the catalytic cycle. For the (IV/III) reduction couple, Table 2, the reactant, $[Ru(IV)-O]^{+2}$, ruthenium has a triplet $t_{2g}^2t_{2g}^1t_{2g}^1$ electron configuration. Given that all octahedral complexes in these calculations have only slightly distorted geometries we expect only slight deviations from 3-fold degenerate t_{2g} orbitals and 2-fold degenerate e_g orbitals. The systematic error of 100 mV for the (III/II) and (IV/III) PCETs shows that B3LYP is making a systematic error of −2.3 kcal/mol in ionizing a single electron from a doubly occupied t_{2g} orbital while simultaneously transferring a second shell proton to a base in water. The results in Tables 1 and 2 show that B3LYP works well for calculating reduction half potentials of PCETs in ruthenium complexes and that it provides the correct energetics for complexes where ruthenium has a high oxidation state as in the catalytically competent species. We have found that for the redox potentials of some other complexes, with metal centers from the first row of the periodic table, B3LYP predicts larger yet systematic errors with respect to experiment.[77]

3.2. PCET and ET Steps for the Catalytic Cycle of Single Site Ruthenium OEC. Table 3 shows a comparison between theory and experiment for the reduction half potentials[11] of the three PCET steps (eqs 1, 2, and 5) and the ET step (eq 3) in the catalytic cycle of the single site ruthenium OECs. In order to investigate the effect of synthetic modification of ligands on the reaction mechanism, as in other structure−activity studies,[11,15,23] three different ligand combinations are considered (mebimpy (2,6-bis(1-methylbenzimidazol-2-yl)pyridine), bpy (2,2′-bipyridine), tpy (2,2′:6′,2″-terpyridine), and mebim-py (3-methyl-1-pyridylbenzimidazol-2-ylidene)).

The last PCET (eq 5) shown in Table 3 was only observed in the cyclic voltammetry experiments[12] for the (mebimpy)(bpm) couple ($[Ru(IV)-OO]^{+2}$ and $[Ru(III)-OOH]^{+2}$) at 1.40 V. The asterisked experimental results shown in Table 3 for the three ligand combinations were estimated from the experimental results of the mebimpy and bpm ligand combination. To accomplish this we estimate the change in a given reduction half potential with a given change in coordinating ligand. This is done by taking the difference between the potential for the $[Ru(III)(mebimpy)(bpm)(OH)]^{+2}$ and $[Ru(II)(mebimpy)(bpm)(H_2O)]^{+2}$ couple (0.97 V)[12] and a given $[Ru(III)(L_1)(L_2)(OH)]^{+2}$ and $[Ru(II)(L_1)(L_2)(H_2O)]^{+2}$ couple. We chose the $[Ru(III)-OH]^{+2}$ and $[Ru(II)-H_2O]^{+2}$ couple as the representative example because these experiments have been extensively studied given that the reaction involves resting state catalyst.[10−12,76] Estimates obtained for each of the three ligand combinations are then subtracted from the (mebimpy)(bpm) couple ($[Ru(IV)-O_2]^{+2}$ and $[Ru(III)-OOH]^{+2}$ at 1.40 V) thereby providing an estimate of the experimental $[Ru(IV)(L_1)(L_2)(O_2)]^{+2}$ and $[Ru(III)(L_1)(L_2)(OOH)]^{+2}$ reduction half potential for each of the three ligand combinations. Based on comparison with other experimental data these estimates are perfectly reasonable, for example they are all less than what is known to be the largest reduction half potential, i.e. the (V/IV) couple and are comparable to the other ruthenium (IV/III) couple for a given ligand combination. Note that the B3LYP results also suggest that the estimated experimental reduction half potentials are reasonable. Literature DFT results[14] for the successive couples of $[Ru(II)(tpy)(bpm)(H_2O)]^{+2}$ at 1.14, 1.31, 1.98, and 1.30 V also suggest that our experimental estimates are reasonable.

Similar to the results obtained using the large database of (III/II) and (IV/III) ruthenium couples in Tables 1 and 2, we see in Table 3 that B3LYP systematically underestimates the reduction half potentials of the complexes therein by about 100 mV. This includes two of three (V/IV) couples with the single remaining (V/IV)

Table 3. Reduction Half Potentials, $E_{1/2}$, from eq 12 of the Three PCET and One ET Steps in the Catalytic Cycle of the Single Site Ruthenium OEC for Three Ligand Combinations[a]

oxidized	reduced	exp./V	B3LYP/V	exp.-B3LYP/V
$[Ru(III)(mebimpy)(bpy)(OH)]^{+2}$	$[Ru(II)(mebimpy)(bpy)(H_2O)]^{+2}$	0.82	0.72	0.10
$[Ru(IV)(mebimpy)(bpy)(O)]^{+2}$	$[Ru(III)(mebimpy)(bpy)(OH)]^{+2}$	1.24	1.12	0.12
$[Ru(V)(mebimpy)(bpy)(O)]^{+3}$	$[Ru(IV)(mebimpy)(bpy)(O)]^{+2}$	1.67	1.58	0.09
$[Ru(IV)(mebimpy)(bpy)(OO)]^{+2}$	$[Ru(III)(mebimpy)(bpy)(OOH)]^{+2}$	*1.25	1.13	0.12
$[Ru(III)(tpy)(bpy)(OH)]^{+2}$	$[Ru(II)(tpy)(bpy)(H_2O)]^{+2}$	1.01	0.94	0.07
$[Ru(IV)(tpy)(bpy)(O)]^{+2}$	$[Ru(III)(tpy)(bpy)(OH)]^{+2}$	1.19	1.14	0.05
$[Ru(V)(tpy)(bpy)(O)]^{+3}$	$[Ru(IV)(tpy)(bpy)(O)]^{+2}$	1.60	2.21	−0.61
$[Ru(IV)(tpy)(bpy)(OO)]^{+2}$	$[Ru(III)(tpy)(bpy)(OOH)]^{+2}$	*1.44	1.28	0.16
$[Ru(III)(tpy)(mebim-py)(OH)]^{+2}$	$[Ru(II)(tpy)(mebim-py)(H_2O)]^{+2}$	1.11	0.96	0.15
$[Ru(IV)(tpy)(mebim-py)(O)]^{+2}$	$[Ru(III)(tpy)(mebim-py)(OH)]^{+2}$	1.49	1.44	0.05
$[Ru(V)(tpy)(mebim-py)(O)]^{+3}$	$[Ru(IV)(tpy)(mebim-py)(O)]^{+2}$	1.70	1.76	−0.06
$[Ru(IV)(tpy)(mebim-py)(OO)]^{+2}$	$[Ru(III)(tpy)(mebim-py)(OOH)]^{+2}$	*1.54	1.59	−0.05

[a] Experimental potentials are from ref 11, and values with asterisks are estimates explained in the Results and Discussion section.

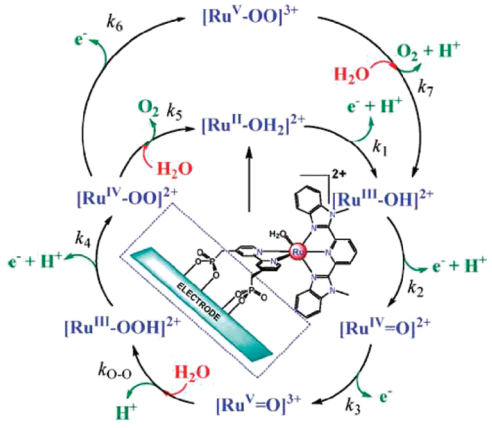

Figure 1. Catalytic cycle of water oxidation using a single site ruthenium OEC.[6,10,40]

couple being a large outlier. We hypothesize that this outlier for the (V/IV) couple of [Ru(tpy)(bpy)(O)] is due to the absence of certain states which are present in the low energy manifold of the Ru(IV) complexes for the other two couples. B3LYP/LACV3P consistently predicts that $[Ru(IV)(tpy)(bpy)(O)]^{+2}$ has only one electronic structure in its low energy manifold of states featuring a doublet oxo ligand bound to ruthenium. As was recently done[66] for spin-splitting energies of transition metal complexes with comparatively simple ligands, addressing the −600 mV outlier more rigorously, necessitates the construction of a large transition metal database containing the comparatively nonstandard and reactive oxo ligand. Otherwise, complexes with oxidation state (II) are $t_{2g}^2t_{2g}^2t_{2g}^2$, (III) are $t_{2g}^2t_{2g}^2t_{2g}^1$, (IV) are $t_{2g}^2t_{2g}^1t_{2g}^1$, and (V) are $t_{2g}^1t_{2g}^1t_{2g}^1$ and so B3LYP is making a systematic error of around −2.3 kcal/mol in ionizing a doubly occupied t_{2g} orbital. The experimental as well as DFT data shows that successive electron removals from transition metals are not terribly different in comparison to some other, for example organic, cases which is a requirement for energetically favorable production of high oxidation state species that increasingly violate the 18 electron rule.

3.3. APT and LE Steps for the Catalytic Cycle of Single Site Ruthenium OEC. The theory literature gives conflicting results for the magnitudes of the activation free energies of the two rate limiting steps (eqs 4 and 6) in the OEC catalytic cycle.[6,12,14] Using DFT cumulative reaction probabilities[14] the activation free energy for the APT step was estimated to be 1.7 kcal/mol, while DFT free energy perturbation methods used in conjunction with transition states from nudged elastic band calculations[6] provided a free energy value around 10 kcal/mol. As will be discussed below, these results are in qualitative disagreement with both each other and with the available experimental data. For the second rate limiting step, i.e. the LE reaction shown in eq 6, the activation free energy has been computed to be 4.4 kcal/mol[14] using a hepta-coordinate transition state featuring O_2 and H_2O both bound to ruthenium. Other DFT calculations,[12] done on the restricted singlet potential energy surface of [Ru(tpy)-(bpm)$(O_2)]^{+2}$, have suggested that this rate limiting reaction may be explained as a large activation free energy of 17.5 kcal/mol required to convert the lower energy $[Ru-\eta^2-O_2]^{+2}$ conformer (0.0 kcal/mol) to the higher energy $[Ru-O-O]^{+2}$ conformer (3.3 kcal/mol).

Calculated activation free energy barriers reported in the literature[6,14] are too small considering recently reported experimental rate constants.[10−12] Rate constants for the APT and LE steps, for example for $[Ru(II)(tpy)(bpm)(H_2O)]^{+2}$, are $k_{OO} = 9.6 \times 10^{-3}$/s and $k_S = 7.4 \times 10^{-4}$/s (see Figure 1), respectively, and as mentioned in the literature[11] the order of these rate limiting steps shows dependence on ligands. Using classical transition state theory with a frequency factor of 10^{11}/s, a value commonly used for solution phase reactions, it is clear that the activation free energy for these two rate limiting reactions needs to be ∼20 kcal/mol for reasonable comparison to experiment, i.e., $10^{-3}-10^{-4}$/s first order rate constants.

More recently a different complex, *cis*-$[Ru(II)(bpy)_2(H_2O)_2]^{+2}$, was studied[39] where one coordinating nitrogen is replaced by a water molecule, for example the common tridentate tpy ligand of $[Ru(II)(tpy)(bpy)H_2O]^{+2}$ is substituted by bpy and water. This complex is interesting because the presence of two waters allows PCETs to result in a catalytically competent bis-oxo intermediate, amounting to a net loss of $4e^-$ and $4H^+$, where ruthenium (Ru(VI)) has a very high oxidation state. This complex features an intramolecular mechanism that is different from those complexes with a RuN_5O core because the water molecule is added across the two catalytically active oxo ligands, where one oxo is responsible for the creation of an O−O bond

dx.doi.org/10.1021/jp2026576 |J. Phys. Chem. B 2011, 115, 9280–9289

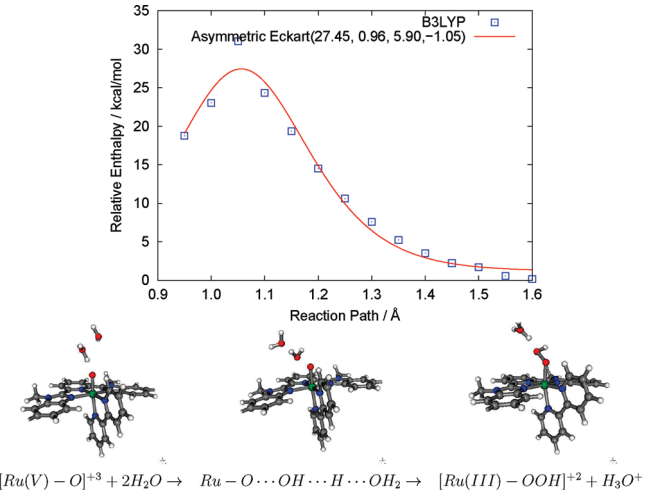

Figure 2. Summary of B3LYP enthalpies and geometries (reactant, transition state, and product) of $[Ru(mebimpy)(bpy)(O)]^{+3}$ for the rate limiting APT step (eq 4) along with a fit of the barrier to the asymmetric Eckhart potential.[83,84] The figure shows the minimum energy path using a reaction path which is simply the OH bond length of the water undergoing proton transfer.

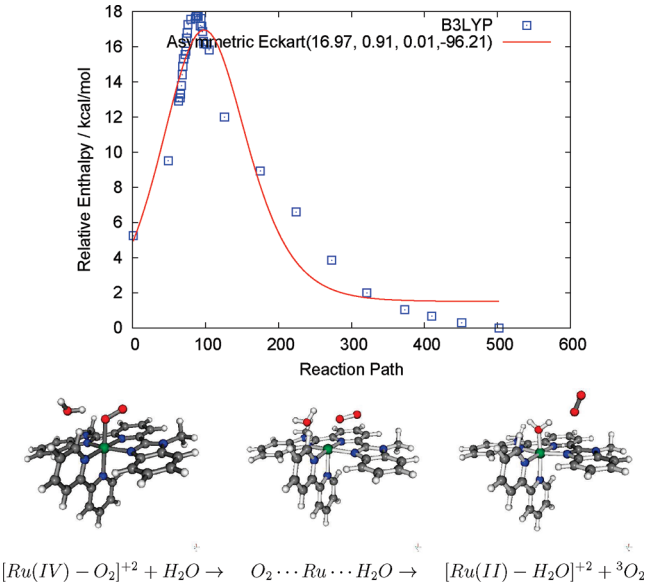

Figure 3. Summary of B3LYP enthalpies and geometries (reactant, transition state, and product) of $[Ru(mebimpy)(bpy)(O_2)]^{+2}$ for the rate limiting LE step (eq 6) along with a fit of the barrier to the asymmetric Eckhart potential.[83,84] The figure shows the minimum energy path using a two-dimensional reaction path of $Ru-O_2$ and $Ru-H_2O$ bond lengths.

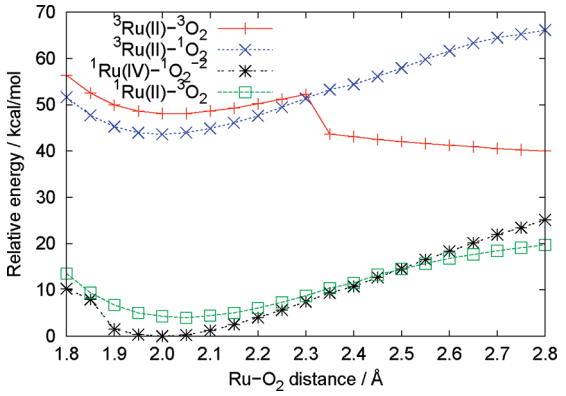

Figure 4. B3LYP bond dissociation energy curves of $[Ru(mebimpy)(bpy)(O_2)]^{+2}$ for four different transition metal wave function guesses. Energies reported are relative to the lowest energy equilibrium point, i.e., for guess $[Ru(IV)-O_2{}^{-2}]^{+2}$. Other guesses are shown in the legend.

while the other oxo acts as a base. This is in contrast to the intermolecular mechanism herein where water passes the proton to a water molecule in solvent. Experimentally, the oxo coordinated base is stronger than water, for example $pK_a^{[Ru(V)(O)(OH)]^{+2}}$ 4.5,[78] while $pK_a^{H_3O^+}$ −1.7. Using the M06-L functional,[79] free energy barriers of 24.5 and 25.1 kcal/mol were determined for the intramolecular APT and LE steps, respectively.[39] The experimental kinetics and barrier heights for water oxidation with *cis*-$[Ru(II)(bpy)_2(H_2O)_2]^{+2}$ are not known.[39,78] The chemistry in this system is quite different from that studied in the present paper, so the results obtained therein cannot be directly compared with those presented here.

There are significant quasi-degeneracies present in $[Ru-O_2]^{+2}$, for example in the $[Ru-O-O]^{+2}$ conformer there are broken symmetry singlet and triplet states at around 3 and 5 kcal/mol lower than the restricted singlet state.[12] The low lying state being a triplet is in agreement with other DFT studies in the literature[14] as well as studies herein. Population of the restricted singlet state may be possible because the previous intermediate $[Ru-\eta^2-O_2]^{+2}$, which has supporting structural information from crystallography,[12] has a broken t_{2g} manifold allowing it to fill restrictively. Although it is possible that the low lying triplet configuration has significant $^3O_2$ character, the triplet character may more likely be on ruthenium, because both experiment[80,81] and B3LYP/LACV3P predict a large triplet to singlet spin-splitting energy for O_2, much larger than the few kcal/mol difference in energy seen between the two conformers. Additionally, B3LYP/LACV3P predicts very large energy differences between $^3O_2$ or $^1O_2$ and $O_2{}^{-2}$, with $O_2{}^{-2}$ having a much larger free energy of solvation and therefore the small energy difference between the two conformers must be for equivalent electronic structures on O_2. This suggests that the restricted singlet wave function is for ruthenium in an excited $t_{2g}^2t_{2g}^2t_{2g}^0$ configuration bound to $O_2{}^{-2}$ and that the low lying triplet state is for ruthenium with a $t_{2g}^2t_{2g}^1t_{2g}^1$ configuration bound to $O_2{}^{-2}$. The broken symmetry singlet lies between these two states. This triplet state is consistent with the experimental spin−orbit coupling constant of around 1000 cm^{-1} for ruthenium complexes and an intersystem crossing mechanism.[12,82]

Intramolecular two-electron transfer on the triplet surface, i.e., from $[^3Ru(IV)-{}^1O_2{}^{-2}]^{+2}$ to $[^1Ru(II)-{}^3O_2]^{+2}$, will be necessary to create $^3O_2$ which will then be replaced with water in the LE step (vide infra).

B3LYP minimum energy paths for the APT and LE rate determining steps in the catalytic cycle of $[Ru(II)(mebimpy)(bpy)(H_2O)]^{+2}$, along with reactant, transition state, and product geometries, are shown in Figures 2 and 3, respectively. The reaction path used for the APT step is simply the OH bond length of the water undergoing the proton transfer while the reaction path used for the LE step is a two-dimensional path involving the $Ru-O_2$ and $Ru-H_2O$ bond lengths. Also included in the figures are fits to the asymmetric Eckhart potential.[83,84] The reaction enthalpies, ΔH^0_{rxn}, are −18.77 kcal/mol and −5.25 kcal/mol for

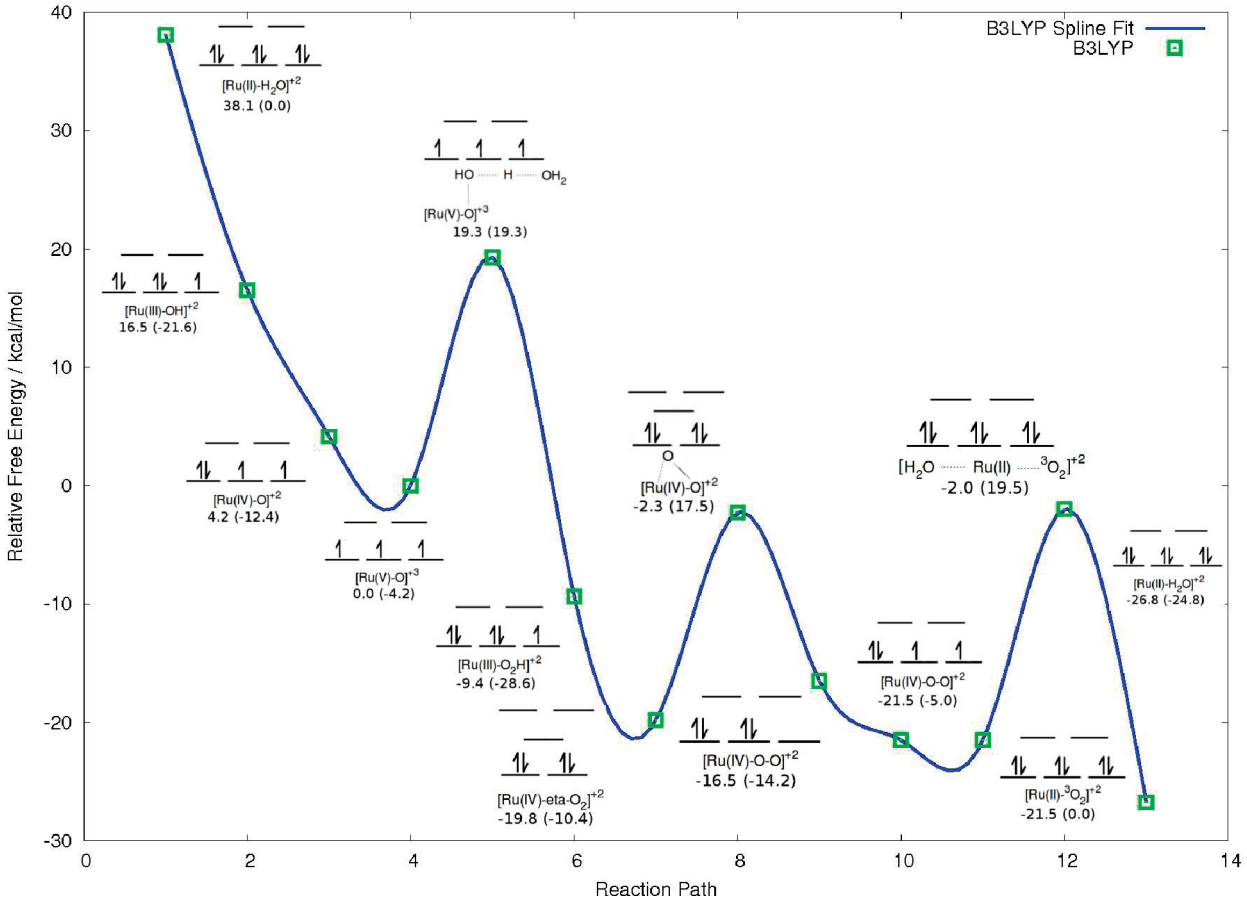

Figure 5. Free energy diagram of the entire water oxidation catalytic mechanism of $[Ru(II)(mebimpy)(bpy)(H_2O)]^{+2}$. All energies are reported in kcal/mol relative to the catalytically competent species, $[Ru(V){-}O]^{+3}$, rather than the precatalyst, $[Ru(II){-}H_2O]^{+2}$. In parentheses are the energy differences between adjacent pairs of points. Ce^{+4} and H_2O contributions to the reaction mechanism are as given in eqs 1−6.

the APT and LE steps, respectively, whereas the activation barriers, $\Delta H^{0\ddagger}$, are 12.27 and 12.53 kcal/mol. The transition states for both reactions require the ordering of a free water molecule which has a translational entropic factor, $\Delta S^{0\ddagger}$, of −25.97 cal/(mol K) according to the Sackur−Tetrode equation and a corresponding "cratic" entropy contribution, $-T\Delta S$ of 7 kcal/mol,[85] leading to a free energy contribution of around 7 kcal/mol at 298 K. For the APT step a water must be taken out of solution and oriented such that the atom transfer step (O−O formation) becomes feasible. In the LE step a water molecule must be taken out of solution to form the hepta-coordinate transition state. The free energies of activation for the rate determining steps, $\Delta G^{0\ddagger}$, become 19.27 and 19.53 kcal/mol for the APT and LE steps respectively, giving excellent agreement with experimental rates constants on the order of 10^{-3}−10^{-4}/s according to classical transition state theory. The B3LYP calculations are able to show that these two steps have roughly equivalent barriers and thus first order rate constants, subject to slightly different orderings depending on coordinating ligands. Entropic contributions to the reaction free energies then become 7 kcal/mol for the APT step and 0 kcal/mol for the LE step resulting in ΔG^0_{rxn} = −11.77 kcal/mol and ΔG^0_{rxn} = −5.25 kcal/mol, respectively.

Figure 4 shows bond dissociation energy curves for O_2 in the $[Ru(mebimpy)(bpy)(O_2)]^{+2}$ complex using four different fragment based transition metal wave function guesses. There are two guesses for $^3O_2$, one bound to low spin singlet Ru(II) and one ferromagnetically bound to intermediate spin triplet Ru(II), there is also a guess for double bonded $^1O_2$ bound to intermediate spin triplet Ru(II), and the last guess is for a higher oxidation state Ru(IV) (singlet) bound to dianionic singlet oxygen. There are other guesses as well but many of those we found to have converged densities that cluster with converged densities from the aforementioned states. For each surface, although there are some conflicting predictions of the partial charges and spin densities obtained using Mulliken, electrostatic potential, and natural atomic orbital[86] analysis methods, overall the electronic structure is best described as $[Ru(II){-}^3O_2]^{+2}$ where two-electrons have been transferred on the triplet potential energy surface, i.e., from the postdeprotonated peroxo species $[^3Ru(IV){-}^1O_2{}^{-2}]^{+2}$ to $[^1Ru(II){-}^3O_2]^{+2}$.[10] In agreement with[12] there are quasi-degeneracies present, for example even though the lowest energy surface belongs to $[^1Ru(II){-}^3O_2]^{+2}$, other calculations have suggested that $[^3Ru(IV){-}^1O_2{}^{-2}]^{+2}$ lies nearby in energy and as shown in Figure 4 the $[^1Ru(IV){-}^1O_2{}^{-2}]^{+2}$ structure lies about 5 kcal/mol higher in energy at the equilibrium geometry. The ground state $^3O_2$ bond dissociation energy is around 20 kcal/mol. Comparing Figures 3 and 4 shows that the incoming water stabilizes the bond dissociation enthalpy by around 8 kcal/mol but an entropic factor of around 7 kcal/mol must be spent to organize the stabilizing water, resulting in the 20 kcal/mol free energy barrier which is consistent with experiment. The excited state curves also

dx.doi.org/10.1021/jp2026576 |J. Phys. Chem. B 2011, 115, 9280–9289

show quasi-degeneracies as well as a curve crossing due to spin contamination.

3.4. Free Energy Diagram for the Catalytic Cycle of Single Site Ruthenium OEC. A summary of the free energies for the entire water oxidation catalytic mechanism of the (mebimpy)(bpy) complex ($[Ru(II)-H_2O]^{+2}$) is presented in Figure 5 where a spline fit of the B3LYP data is included for clarity. The energies are reported relative to the catalytically competent species, $[Ru(V)-O]^{+3}$, rather than the resting state precatalyst, $[Ru(II)-H_2O]^{+2}$. These energies take into account the experimental reduction half potential of cerium, $Ce^{+4} + e^- \rightarrow Ce^{+3}$, at 1.76 V as well as the experimental free energy of protonation of water, $H_2O + H^+ \rightleftharpoons H_3O^+$, at 2.37 kcal/mol ($\Delta G = 2.303RT\,pK_a^{H_3O^+}$), according to eqs 1−6. The water oxidation half reaction in eq 7 has a potential of −1.23 V giving a reaction free energy of −12.2 kcal/mol according to the Nernst equation (eq 10) while the B3LYP reaction free energy from Figure 5 is −26.8 kcal/mol. Their difference is subject to accumulative B3LYP errors due to various aspects of the catalytic mechanism, for example the errors due to quasi-degeneracies, treatment of the cerium potential, etc., as well as errors in the experimental data. As mentioned previously, many quasi-degeneracies are present in the later part of the curve, i.e., for points 7, 9, 10, and 11, consistent with the intersystem crossing between the restricted singlet (point 9) and the triplet (point 10), both in the present study and in the literature.[12] With these quasi-degeneracies a concerted mechanism, as opposed to a stepwise mechanism, where the last two barriers (17.5 and 19.5 kcal/mol) are combined into one is certainly feasible.

4. CONCLUSION

PCET, ET, APT, and LE reactions in the catalytic cycle of single site ruthenium water oxidation have been investigated using B3LYP/LACV3P with continuum solvent and new protocols that allow greater flexibility in sampling different electronic configurations via suitable initial guess wave functions. MUEs with respect to experiment and standard deviations for reduction half potentials calculated with our protocol compare favorably with alternative calculations in the literature. The calculation of reduction half potentials for a large database of (III/II) and (IV/III) ruthenium couples with different ligand combinations shows that B3LYP systematically underestimates experimental values by only 100 mV which is taken as the inherent error in B3LYP's ionization of a doubly occupied t_{2g} orbital. For the rate limiting APT and LE steps our energetics, $\Delta G^{0\ddagger} = 19.27$ kcal/mol for APT and $\Delta G^{0\ddagger} = 19.53$ kcal/mol for LE, provide excellent agreement with experimental rate constants. Considering the quasi-degenerate surface toward the end of the catalytic mechanism, the recently discussed $[Ru-\eta-O_2]^{+2} \rightarrow [Ru-O-O]^{+2}$ barrier[12] prior to LE, may be combined with the LE barrier giving a concerted mechanism. These results provide quantitative support for the model of the catalytic cycle which has been advanced in several experimental papers, and provide a foundation for theoretically exploring the rate constants that might be obtained from ligand substitutions and other changes in the catalytic system.

AUTHOR INFORMATION

Corresponding Author

*E-mail: rich@chem.columbia.edu.

ACKNOWLEDGMENT

T.F.H. thanks Javier Concepcion and Lee-Ping Wang for supplying geometries of ruthenium complexes. This work has been supported by the Department of Energy program through solar photochemistry (DE-FG02-90ER-14162) to R.A.F.

REFERENCES

(1) Ferreira, K.; Iverson, T.; Maghlaoui, K.; Barber, J.; Iwata, S. *Science* **2004**, *303*, 1831.
(2) Debus, R. *Biochim. Biophys. Acta* **1992**, *1102*, 269.
(3) Styring, S. *Chem. Soc. Rev.* **2001**, *30*, 36.
(4) Ananyev, G. M.; Zaltsman, L.; Vasko, C.; Dismukes, G. C. *Biochim. Biophys. Acta* **2001**, *1503*, 52.
(5) Meyer, T. J.; Huynh, M. H. V.; Thorp, H. H. *Angew. Chem., Int. Ed. Engl.* **2007**, *46*, 5284.
(6) Chen, Z.; Concepcion, J. J.; Hu, X.; Yang, W.; Hoertz, P. G.; Meyer, T. J. *Proc. Natl. Acad. Sci.* **2010**, *107*, 7225.
(7) Siegbahn, P.; Crabtree, R. *J. Am. Chem. Soc.* **1999**, *121*, 117.
(8) Vrettos, J.; Limburg, J.; Brudvig, G. *Biochim. Biophys. Acta* **2001**, *1503*, 229.
(9) Chen, Z.; Concepcion, J. J.; Hull, J. F.; Hoertz, P. G.; Meyer, T. J. *Dalton Trans.* **2010**, *39*, 6950.
(10) Concepcion, J. J.; Jurss, J. W.; Brennaman, M. K.; Hoertz, P. G.; Patrocinio, A. O. T.; Iha, N. Y. M.; Templeton, J. L.; Meyer, T. J. *Acc. Chem. Res.* **2009**, *42*, 1954.
(11) Concepcion, J. J.; Jurss, J. W.; Norris, M. R.; Chen, Z.; Templeton, J. L.; Meyer, T. J. *Inorg. Chem.* **2010**, *49*, 1277.
(12) Concepcion, J. J.; Tsai, M.-K.; Muckerman, J. T.; Meyer, T. J. *J. Am. Chem. Soc.* **2010**, *132*, 1545.
(13) Concepcion, J.; Jurss, J.; Templeton, J.; Meyer, T. *J. Am. Chem. Soc.* **2008**, *130*, 16462.
(14) Wang, L.-P.; Wu, Q.; Van Voorhis, T. *Inorg. Chem.* **2010**, *49*, 4543.
(15) Tseng, H.; Zong, R.; Muckerman, J.; Thummel, R. *Inorg. Chem.* **2008**, *47*, 11763.
(16) Meyer, T. J. *Acc. Chem. Res.* **1989**, *22*, 163.
(17) Wasielewski, M. R. *Chem. Rev.* **1992**, *92*, 435.
(18) Gratzel, M. *Acc. Chem. Res.* **1981**, *14*, 376.
(19) Bard, A. J.; Fox, M. A. *Acc. Chem. Res.* **1995**, *28*, 141.
(20) Lewis, N. S.; Nocera, D. G. *Proc. Natl. Acad. Sci.* **2006**, *103*, 15729.
(21) Muckerman, J. T.; Polyansky, D. E.; Wada, T.; Tanaka, K.; Fujita, E. *Inorg. Chem.* **2008**, *47*, 1787.
(22) Kohl, S. W.; Weiner, L.; Schwartsburd, L.; Konstantinovski, L.; Shimon, L. J. W.; Ben-David, Y.; Iron, M. A.; Milstein, D. *Science* **2009**, *324*, 74.
(23) Wasylenko, D. J.; Ganesamoorthy, C.; Henderson, M. A.; Koivisto, B. D.; Osthoff, H. D.; Berlinguette, C. P. *J. Am. Chem. Soc.* **2010**, *132*, 16094.
(24) Jurss, J. W.; Concepcion, J. C.; Norris, M. R.; Templeton, J. L.; Meyer, T. J. *Inorg. Chem.* **2010**, *49*, 3980.
(25) Liu, F.; Concepcion, J.; Jurss, J.; Cardolaccia, T.; Templeton, J.; Meyer, T. *Inorg. Chem.* **2008**, *47*, 1727.
(26) Lebeau, E.; Adeyemi, S.; Meyer, T. *Inorg. Chem.* **1998**, *37*, 6476.
(27) Yang, X.; Baik, M.-H. *J. Am. Chem. Soc.* **2008**, *130*, 16231.
(28) Xu, Y.; Akermark, T.; Gyollai, V.; Zou, D.; Eriksson, L.; Duan, L.; Zhang, R.; Akermark, B.; Sun, L. *Inorg. Chem.* **2009**, *48*, 2717.
(29) Wada, T.; Tsuge, K.; Tanaka, K. *Inorg. Chem.* **2001**, *40*, 329.
(30) Seidler-Egdal, R. K.; Nielsen, A.; Bond, A. D.; Bjerrumb, M. J.; McKenzie, C. J. *Dalton Trans.* **2011**, *40*, 3849.
(31) Li, G.; Sproviero, E. M.; McNamara, W. R.; Snoeberger, R. C., III; Crabtree, R. H.; Brudvig, G. W.; Batista, V. S. *J. Phys. Chem. B* **2010**, *114*, 14214.
(32) Ellis, W. C.; McDaniel, N. D.; Bernhard, S.; Collins, T. J. *J. Am. Chem. Soc.* **2010**, *132*, 10990.
(33) McAlpin, J. G.; Surendranath, Y.; Dincă, M.; Stich, T. A.; Stoian, S. A.; Casey, W. H.; Nocera, D. G.; Britt, R. D. *J. Am. Chem. Soc.* **2010**, *132*, 6882.

(34) Yin, Q.; Tan, J. M.; Besson, C.; Geletii, Y. V.; Musaev, D. G.; Kuznetsov, A. E.; Luo, Z.; Hardcastle, K. I.; Hill, C. L. *Science* **2010**, *328*, 342.
(35) Karunadasa, H. I.; Chang, C. J.; Long, J. R. *Nature* **2010**, *464*, 1329.
(36) Dzik, W. I.; Calvo, S. E.; Reek, J. N. H.; Lutz, M.; Ciriano, M. A.; Tejel, C.; Hetterscheid, D. G. H.; de Bruin, B. *Organomatallics* **2011**, *30*, 372.
(37) Winther-Jensen, O.; Winther-Jensen, B.; MacFarlane, D. R. *Electrochem. Commun.* **2011**, *13*, 307.
(38) Nam, Y. S.; Magyar, A. P.; Lee, D.; Kim, J.-W.; Yun, D. S.; Park, H.; Pollom, T. S., Jr.; Weitz, D. A.; Belcher, A. M. *Nat. Nanotechnol.* **2010**, *5*, 340.
(39) Sala, X.; Ertem, M. Z.; Vigara, L.; Todorova, T. K.; Chen, W.; Rocha, R. C.; Aquilante, F.; Cramer, C. J.; Gagliardi, L.; Llobet, A. *Angew. Chem., Int. Ed. Engl.* **2010**, *49*, 7745.
(40) Chen, Z.; Concepcion, J. J.; Luo, H.; Hull, J. F.; Paul, A.; Meyer, T. J. *J. Am. Chem. Soc.* **2010**, *132*, 17670.
(41) Yang, X.; Hall, M. B. *J. Am. Chem. Soc.* **2010**, *132*, 120.
(42) Creutz, C.; Chou, M. H.; Hou, H.; Muckerman, J. T. *Inorg. Chem.* **2010**, *49*, 9809.
(43) Wasylenko, D. J.; Ganesamoorthy, C.; Koivisto, B. D.; Henderson, M. A.; Berlinguette, C. P. *Inorg. Chem.* **2010**, *49*, 2202.
(44) Yu, H.; Fu, Y.; Guo, Q.; Lin, Z. *Organomatallics* **2009**, *28*, 4443.
(45) Chen, Y.; Fang, W. H. *J. Phys. Chem. A* **2010**, *114*, 10334.
(46) Nyhlén, J.; Duan, L.; Åkermark, B.; Sun, L.; Privalov, T. *Angew. Chem., Int. Ed. Engl.* **2010**, *49*, 1773.
(47) Tong, L.; Duan, L.; Xu, Y.; Privalov, T.; Sun, L. *Angew. Chem., Int. Ed. Engl.* **2011**, *50*, 445.
(48) Paulsen, H.; Duelund, L.; Winkler, H.; Tolflund, H.; Trautwein, A. X. *Inorg. Chem.* **2001**, *40*, 2201.
(49) Jensen, K. P.; Cirera, J. *J. Phys. Chem. A* **2009**, *113*, 10033.
(50) Reiher, M. *Inorg. Chem.* **2002**, *41*, 6928.
(51) Liao, M.-S.; Huang, M.-J.; Watts, J. D. *J. Phys. Chem. A* **2010**, *114*, 9554.
(52) Takatani, T.; Sears, J. S.; Sherrill, C. D. *J. Phys. Chem. A* **2010**, *114*, 11714.
(53) Carreón-Macedo, J.-L.; Harvey, J. N. *Phys. Chem. Chem. Phys.* **2006**, *8*, 93.
(54) Conradie, J.; Ghosh, A. *J. Phys. Chem. B* **2007**, *111*, 12621.
(55) Swart, M.; Groenhof, A. R.; Ehlers, A. W.; Lammertsma, K. *J. Phys. Chem. A* **2004**, *108*, 5479.
(56) Deeth, R. J.; Anastasi, A. E.; Wilcockson, M. J. *J. Am. Chem. Soc.* **2010**, *132*, 6876.
(57) Zhao, Y.; Schultz, N.; Truhlar, D. *J. Chem. Theory Comp.* **2006**, *2*, 364.
(58) Gonzalez-Blanco, O.; Branchadell, V. *J. Chem. Phys.* **1999**, *110*, 778.
(59) Wu, Z. *Chem. Phys. Lett.* **2004**, *383*, 251.
(60) Roy, L. E.; Jakubikova, E.; Guthrie, M. G.; Batista, E. R. *J. Phys. Chem. A* **2009**, *113*, 6745.
(61) Uudsemaa, M.; Tamm, T. *J. Phys. Chem. A* **2003**, *107*, 9997.
(62) Galstyan, A.; Knapp, E.-W. *J. Comput. Chem.* **2009**, *30*, 203.
(63) Baik, M.-H.; Friesner, R. A. *J. Phys. Chem. A* **2002**, *106*, 7407.
(64) Vacek, G.; Perry, J. K.; Langlois, J.-M. *Chem. Phys. Lett.* **1999**, *310*, 189.
(65) Jaguar, version 7.5; Schrödinger, Inc.: New York, NY.
(66) Hughes, T. F.; Friesner, R. A. *J. Chem. Theory Comp.* **2011**, *7*, 19.
(67) Maestro, version 8.5; Schrödinger, Inc.: New York, NY.
(68) Lee, C.; Yang, W.; Parr, R. *Phys. Rev. B* **1988**, *37*, 785.
(69) Becke, A. *J. Chem. Phys.* **1993**, *98*, 5648.
(70) Rinaldo, D.; Tian, L.; Harvey, J.; Friesner, R. A. *J. Chem. Phys.* **2008**, *129*, 164108.
(71) Hay, P. J.; Wadt, W. R. *J. Chem. Phys.* **1985**, *82*, 299.
(72) Lippstreu, J.; Straub, B. *J. Am. Chem. Soc.* **2005**, *127*, 7444.
(73) O'Brien, J.; Williams, E. *J. Phys. Chem. A* **2008**, *112*, 5893.
(74) Friesner, R.; Murphy, R.; Beachy, M.; Ringnalda, M.; Pollard, W.; Dunietz, B.; Cao, Y. *J. Phys. Chem. A* **1999**, *103*, 1913.
(75) Peng, C.; Schlegel, H. *Israel J. Chem.* **1993**, *33*, 449.
(76) Dovletoglou, A.; Adeyemi, S. A.; Meyer, T. J. *Inorg. Chem.* **1996**, *35*, 4120.
(77) Hughes, T. F.; Friesner, R. A. in preparation.
(78) Dobson, J. C.; Meyer, T. J. *Inorg. Chem.* **1988**, *27*, 3283.
(79) Zhao, Y.; Truhlar, D. G. *J. Chem. Phys.* **2006**, *125*, 194101.
(80) Schmitt, R.; Bierbaum, V.; DePuy, C. *J. Am. Chem. Soc.* **1979**, *101*, 6443.
(81) Yamaguchi, K.; Jensen, F.; Dorigo, A.; Houk, K. N. *Chem. Phys. Lett.* **1988**, *149*, 537.
(82) Srnec, M.; Chalupský, J.; Fojta, M.; Zendlová, L.; Havran, L.; Hocek, M.; Kývala, M.; Rulíšek, L. *J. Am. Chem. Soc.* **2008**, *130*, 10947.
(83) Miller, W. H.; Zhao, Y.; Ceotto, M.; Yang, S. *J. Chem. Phys.* **2003**, *119*, 1329.
(84) The asymmetric Eckhart potential

$$V(x) = \frac{V_0(1-\alpha)}{1+e^{-2a(x+c)}} + \frac{V_0(1+\sqrt{\alpha})^2}{4\,cosh^2(a(x+c))}$$

with parameters V_0, α, a, and c (given in the same order in the legends of Figures 2 and 3) being a potential commonly used to model dynamics of chemical reactions.
(85) Hermans, J.; Wang, L. *J. Am. Chem. Soc.* **1997**, *119*, 2707.
(86) Reed, A.; Weinstock, R.; Weinhold, F. *J. Chem. Phys.* **1985**, *83*, 735.